Dyes and Pigments 92 (2011) 563–572

Contents lists available at ScienceDirect

Dyes and Pigments

journal homepage: www.elsevier.com/locate/dyepig

Evaluating the effectiveness of photocatalysts based on titanium dioxide in the degradation of the dye Ponceau 4R

Danielle F.M. Oliveira [a], Paulo S. Batista [a,d], Paulo S. Muller Jr. [b], Valdemir Velani [b], Marcela D. França [a], Danilo R. de Souza [a,c], Antonio E.H. Machado [a,d,*]

[a] Instituto de Química, Universidade Federal de Uberlândia, Caixa Postal 593, 38400-902 Uberlândia, MG, Brazil
[b] Nanobrax, Soluções Tecnológicas e Prestação de Serviços Ltda, 38400-608 Uberlândia, MG, Brazil
[c] Instituto de Ciências Ambientais e Desenvolvimento Sustentável, Universidade Federal da Bahia, 47805-100 Barreiras, Ba, Brazil
[d] Departamento de Química, Campus Catalão Universidade Federal de Goiás, 75704-020 Catalão, Go, Brazil

ARTICLE INFO

Article history:
Received 2 March 2011
Received in revised form
30 May 2011
Accepted 2 June 2011
Available online 21 June 2011

Keywords:
TiO_2 photocatalysts
TiO_2/zinc phthalocyanine composite
AOP
Photodegradation
Ponceau 4R
DFT

ABSTRACT

The performance of different titanium dioxide (TiO_2) catalysts and a composite based on the association between TiO_2 P25 and Zinc Phthalocyanine (TiO_2/ZnPc 1.6%) was evaluated in the photocatalytic degradation of the dye Ponceau 4R (C.I. 16255). The results show that the composite presents a better performance than the other, reaching about 50% mineralization of the dye in 120 min of reaction, around three times higher than that observed under the action of pure TiO_2 P25, although this catalyst presents a quantum yield of hydroxyl radical generation about three times higher than that estimated for the composite. This result seems to be a consequence of the synergism between the electronically excited ZnPc aggregates and the TiO_2 surface.

A parallel study, based on methods from quantum mechanics also suggested the most feasible routes for the photodegradation of the dye in the absence of the catalyst.

1. Introduction

The environmental impact caused by the discharge of pollutants into rivers and lakes is becoming increasingly worrying. A highly frequent consequence is the death of fish and other aquatic organisms. Furthermore, effects such as bioaccumulation and subsequent penetration of toxic compounds in the food chain of aquatic organisms have been routinely detected. Such situations have led to serious ecological problems and consequences for health and human welfare and for quality of life on the planet [1–4].

In general, the discharge of wastewaters containing synthetic dyes tends to cause serious damage to aquatic biota, with direct implications on photosynthesis and oxygenation, in addition to the usual toxicity of these compounds and resistance to natural degradation [1,5–9]. As result, there has been a great effort toward the development of alternative technologies aiming at the destruction of contaminants present in biorecalcitrant wastewater before discharge. In this context, Advanced Oxidation Processes (AOP) are becoming an increasingly important alternative [1,6–8,10,11–14]. Among the AOP, we highlight the heterogeneous photocatalytic processes. In general, heterogeneous photocatalytic processes involve the electronic excitation of a semiconductor oxide such as titanium dioxide (TiO_2), with a band-gap in the UV-A, resulting in the generation of electron/hole pairs [7,13,14]. Through sequences of chain reactions, primarily initiated by free radicals such as the hydroxyl radical and superoxide anion radical [1,7,13,14], the organic matter in effluents (liquid, solid or gaseous) can be oxidized until its mineralization. Titanium dioxide is one of the most commonly used semiconductor oxides in environmental photocatalysis, being of low toxicity, insoluble in water, relatively low cost, with good capacity for reuse, stable to photo and chemical corrosion over a wide range of pH [3,4,7].

Although the mechanism of photocatalytic processes based on the action of semiconductor oxides is not completely understood, some aspects are already well accepted. The absorption, by TiO_2, of energy in the UV-A capable of electronic excitation, leads to the promotion of electrons from the valence band (VB) to the conduction band (CB) [7,13,15]. At the VB the formation of electron-deficient regions (holes, $h+$) occurs, capable of generating hydroxyl

* Corresponding author. Instituto de Química, Universidade Federal de Uberlândia, Caixa Postal 593, 38400-902 Uberlândia, MG, Brazil. Tel.: +55 34 3239 4428; fax: +55 34 3239 4208.
E-mail address: aeduardo@ufu.br (A.E.H. Machado).

0143-7208/$ – see front matter © 2011 Elsevier Ltd. All rights reserved.
doi:10.1016/j.dyepig.2011.06.007

radicals via reaction with substrates such as water, hydroxide ions and hydrogen peroxide, in the surrounding medium. These holes have pH dependent and strongly positive electrochemical potentials (+1.0 to +3.5 V vs. Normal Hydrogen Electrode, NHE), allowing the oxidation of a large number of molecules [7,13]. Hydroxyl radicals can be formed from hydroxide ions or water molecules adsorbed onto the semiconductor surface through electron transfer reactions between these species and the holes, causing the electron-deficient regions from the valence band to return to the previous condition [15,16]. On the other hand, if the kinetic control of these processes is not possible, electron/hole recombination tends to be the predominant process, compromising photocatalytic activity [7,13].

The electrons transferred to the conduction band are responsible for the reduction reactions due to the potential lying between +0.5 and −1.0 V [7]. This band can mediate the reduction of inorganic ions, but can also generate important oxidant species, such as the superoxide anion radical and hydrogen peroxide.

The adsorption step, in TiO_2, of the substances to be reduced and oxidized is crucial for the photocatalytic process, since these species contribute to minimize the tendency of electron/hole recombination [7,13,15]. The adsorption process is governed by electrostatic forces established between the surface of the photocatalyst and the substrate. The pH of the medium determines the surface charge of TiO_2. For TiO_2 P25 Degussa, the zero point charge pH (pH_{zpc}) is equal to 6.25 [13], while for anatase this value is around 4 [17]. At pH lower than pH_{zpc} the surface of the photocatalyst will have positive charge, favoring the adsorption of negatively charged substrates, and its consequent degradation. At pH higher than pH_{zpc} the adsorption of positively-charged substrates is favored [13,15].

The band gap energy of titanium dioxide and its photocatalytic activity is strongly correlated to particle morphology, proportion and distribution of their polymorphic forms and dispersion of photocatalytic sites [18,19]. The control of these parameters may define features which tend to be advantageous to the photocatalytic activity of semiconductors, such as a high surface area, size uniformity and regularity of particle shape, internal porosity, and especially crystal lattice defects, that contribute to a lower rate of electron-hole recombination [7,13,20].

TiO_2 P25, frequently used as a reference in studies of heterogeneous photocatalysis, has a band gap energy around 3.2 eV [2,7,13,14]. This oxide is made up of nanoparticles comprising a range of sizes between 30 and 50 nm and a relatively large surface area, around 52 m^2/g. These parameters along with their average composition, 70% anatase and rutile 30%, seem to guarantee the occurrence of crystal defects that can slow the natural recombination of charge carriers, allowing the material to exhibit a high photocatalytic activity.

TiO_2 photocatalytic activity may have improved by its association with species such as certain photosensitizer dyes that can be electronically excited by low energy photons, making possible the electron transfer from these species to semiconductor conduction band, thus increasing the charge carrier concentration load beyond that obtained through direct electronic excitation of the semiconductor [14,21–23].

Ponceau 4R (P4R), or trisodium (8Z)-7-oxo-8-[(4-sulpho natonaphthalen-1-yl)hydrazinylidene]naphthalene-1,3-disulphonate (Fig. 1) is an azo-dye employed in the food industry to give red coloring to foods. This dye is classified as a carcinogen in some countries including the United States, Norway and Finland, and is currently listed as a banned substance by U.S. Food and Drug Administration (FDA) [24]. A relatively recent study, funded by the Food Standards Agency (United Kingdom) found that P4R when used in combination with other food colorings and preservatives induced an increase in hyperactivity in children [25]. Moreover, because P4R is an azo dye, it can cause intolerance in persons allergic to salicylates. This dye is also known to be histamine-releasing, and may intensify symptoms of asthma in susceptible people [25].

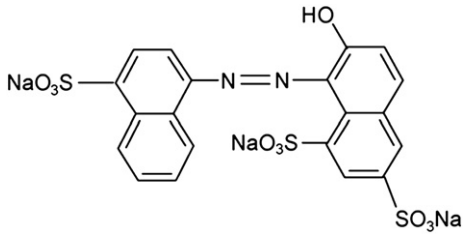

Fig. 1. Chemical structure of Ponceau 4R in the neutral form.

The European Food Safety Authority (EFSA) recently decided to reduce the acceptable daily dose of P4R from 4 mg/kg to 0.7 mg/kg by body mass, in view of the health risks entailed by its use [26].

In this paper, we report the photocatalytic degradation of P4R promoted by TiO_2 prepared by different ways and a composite based on the association between Degussa P25 TiO_2 and zinc phthalocyanine, and the superior performance of the latter compared to the others.

2. Experimental

2.1. Reagents and catalysts

Acidified aqueous solutions (pH 3.0) of Ponceau 4R (Acid red 18, C.I. 16255, Sigma-Aldrich, dye content = 80%) were used in this study as model effluent, at a concentration of 4.0×10^{-5} mol L^{-1} in terms of dye content. Its chemical structure is shown in Fig. 1.

The following catalysts were evaluated in this study: TiO_2 Degussa P25, TiO_2/ZnPc 1.6% composite, TiO_2 Pechini 1:2:8, TiO_2 Pechini 1:4:16, TiO_2 Pechini 1:8:32 and TiO_2 Sol–Gel TX. The preparation procedures are presented below.

The composite TiO_2/ZnPc 1.6% was prepared using methods previously described [14], which consists in the adsorption of 1.6% (w/w) of zinc phthalocyanine in the TiO_2 Degussa P25.

TiO_2 P25 Degussa was kindly provided by Dr. Christian Sattler (DLR (German Aerospace Center) – Institute of Technical Thermodynamics, Solar Research, Köln, Germany).

The Pechini TiO_2 was prepared by the following procedure: initially, titanium tetraisopropoxide (TIT) was dissolved in ethylene glycol (EG) under stirring at 60 °C. After solubilization, citric acid (CA) was added and the reaction temperature was raised to 90 °C. To obtain the powders of TiO_2, the material was submitted to a thermal treatment in two stages: at 110 °C for 1 h (polymerization step), and calcination at 450 °C for 2 h. The heating rate in the two levels of temperature was 10 °C min^{-1}. This catalyst was prepared in three different molar ratios between the reactants (TIT:CA:EG) in the precursor solution (1:2:8; 1:4:16 and 1:8:32).

TiO_2 sol–gel was obtained by the following procedure: solution A, an aqueous of nitric acid (pH = 1.0), was slowly added to solution B, titanium tetraisopropoxide in 2-propanol, whose TIT/2-propanol molar ratio was fixed at 1:4. The solution A/Solution B molar ratio was fixed as being 10:1. The resulting mixture was kept under vigorous stirring for 1 h with the aid of a Tecnal, model TE-139 mechanical stirrer, with the simultaneous application of ultrasound. At the end of stirring, the mixture was kept at rest for approximately 12 h. The excess of solvent was then evaporated with the aid of a flow of hot air. The resulting mass was heated at a heating rate of 5 °C/min, and annealed for 1 h at 100 °C. Then the temperature was raised to 450 °C at a rate of 20 °C/min and maintained at this temperature for 5 h.

2.2. Procedures

Two sets of experiments were performed: direct photolysis of the solution containing the dye (control) and photolysis in the presence of a catalyst. In the second case, a catalyst concentration of 100 mg L^{-1} was used, since the gain with increasing catalyst concentration in a range between 100 and 1000 mg L^{-1} is minimal [2].

The experiments were performed on a laboratory scale, using as irradiation source a 400 W high pressure mercury vapor lamp. About 4 liters of the model effluent were used in each experiment.

The effluent to be photolysed was transferred to a reservoir with a capacity of 8 l, which feeds, by pumping, the photocatalytic reactor at a constant rate of 1350 ml/min (Fig. 2). Aliquots of effluent were collected every 20 min of reaction, for a maximum period of 120 min of photolysis. The aliquot corresponding to $t = 0$ was collected after a 5 min period of circulation of the effluent prior to initiating the photolysis, for homogenization of the mixture to be photolysed. All experiments were performed at least in triplicate.

The photocatalytic reactor consists of an annular container of borosilicate glass, with jacket 1 cm optical path through which the material flows to be photolysed. The high pressure mercury vapor lamp was positioned in the center of the container. The photonic flux provided by the lamp, considering a range of wavelengths between 295 and 710 nm, was estimated to be equal to 3.3×10^{-6} einstein/s [14], with an average dose of 1100 W/m^2 of UVA radiation emitted by this lamp [27].

During the experiments the pH of aliquots taken during the reactions was monitored. There were no significant changes in either experiment.

Despite the photonic activation of the catalyst occurring at considerably high rates, excessive heating of the reaction medium can affect the adsorption of the substrate to be degraded [27]. Because of this, it is necessary to control the temperature of the reaction medium to ensure efficient degradation. Thus, in this study, the temperature of the reaction medium was maintained at 40 ± 2 °C by a cooling system positioned between the reservoir and pump (Fig. 2).

The aliquots collected in the experiments in the presence of the catalyst were filtered using Millipore filters (0.45 μm of mean pore size) to remove suspended TiO_2. All photolysed samples underwent the following tests: pH monitoring, spectrophotometric measurements through the use of a UV/VIS dual beam Shimadzu UV-1650PC spectrophotometer, and measurements of Total Organic Carbon (TOC) using a Shimadzu (TOC-VCPH) Total Organic Carbon Analyzer.

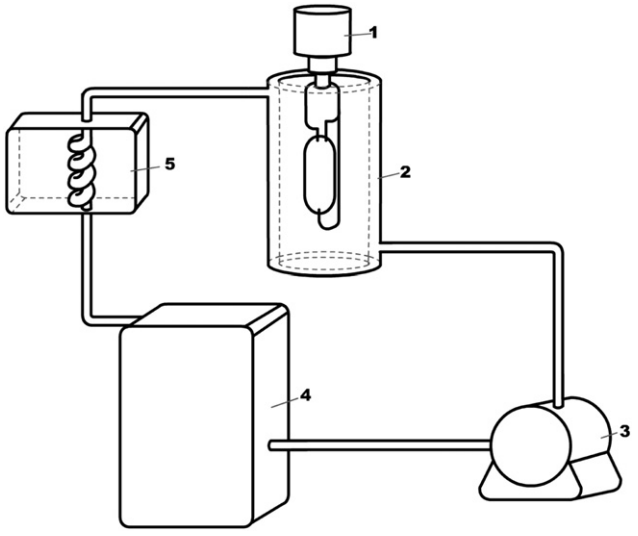

Fig. 2. Schematic representation of the photochemical system employed at laboratory scale: 1 – Irradiation source (Hg lamp); 2 – reactor; 3 – hydraulic pump; 4 – reservoir; 5 – cooler.

P4R decolorization during the photolysis was monitored spectrophotometrically, taking as a reference the wavelength at 507 nm of the absorption spectra of P4R in aqueous medium, where the dye presents an intense absorption band. The percentage of dye decolorization was estimated using the following equation.

$$\%D = \left(1 - \frac{A_t}{A_0}\right) \times 100$$

In which A_t is the absorbance of the aqueous solution of P4R at 507 nm after t minutes of photolysis and A_0 is the absorbance before photolysis.

2.2.1. Estimation of hydroxyl radical production by the composite TiO_2/FtZn 1.6%

For the tests aiming to estimate the quantum yield of hydroxyl radical production, an adaptation of the procedure proposed by Gao et al. [28] was used, as previously described [14].

2.2.2. Measurement of specific surface area and estimate the percentage of anatase in the studied oxides

The measurement of specific surface area of catalysts was carried out using a Quantachrome Nova 1200 equipment, from the adsorption of nitrogen gas. In these experiments 1.0 g of previously dried material was used per sample.

The oxides used in this study were characterized by X-ray diffraction with the aid of a Shimadzu XRD-6000 diffractometer, using a CuKα ($\lambda = 1.54148$ nm) monochromatic source with angular interval $10° \leq 2\theta \leq 90°$. The step count was 0.02°, with counting time of 3 s. The collected data were used to evaluate the composition of the oxides. Crystalline silicon was used as diffraction standard. The crystalline phase was defined by comparison with the JCPDS crystallographic forms [29].

2.2.3. Theoretical simulations

In order better to describe the structure of solvated P4R, a theoretical model involving the ionized structure of the dye enveloped by discrete molecules of water and H_3O^+ ions was adopted (Fig. 3). These molecules and ions perform discrete interactions with the dye in combination with a self-consistent reaction field defined by IEFPCM (Integral Equation Formalism of Polarized Continuum Solvation Method) [30]. The water molecules and the H_3O^+ ions were introduced to improve the description of the solvated environment by introducing specific interactions not described by the IEFPCM.

The optimization of this set of chemical species in the ground state, was based on the use of hybrid functional B3LYP from Density Functional Theory (DFT) in combination with the 6-31G(d,p) atomic basis set. Infrared frequency calculations confirmed the set of chemical species representative of a structure of global minimum energy.

From the structure of minimum energy, the electronic spectrum was simulated for the first 25 singlet excited states. The structure of the first singlet excited state was optimized using the time-dependent version of the same theory (TD-DFT). Additionally, from calculations based on semi-empirical PM6 model, we estimated the minimum energy required to promote the homolytic cleavage in different positions of P4R, in the ground state and for the relaxed S_1. In the semi-empirical calculations, COSMO (Conductor-like Screening Model) [31] was used as continuous dielectric model.

Analysis of the results was able to suggest how the degradation of P4R, viewed through decolorization via direct photolysis, can

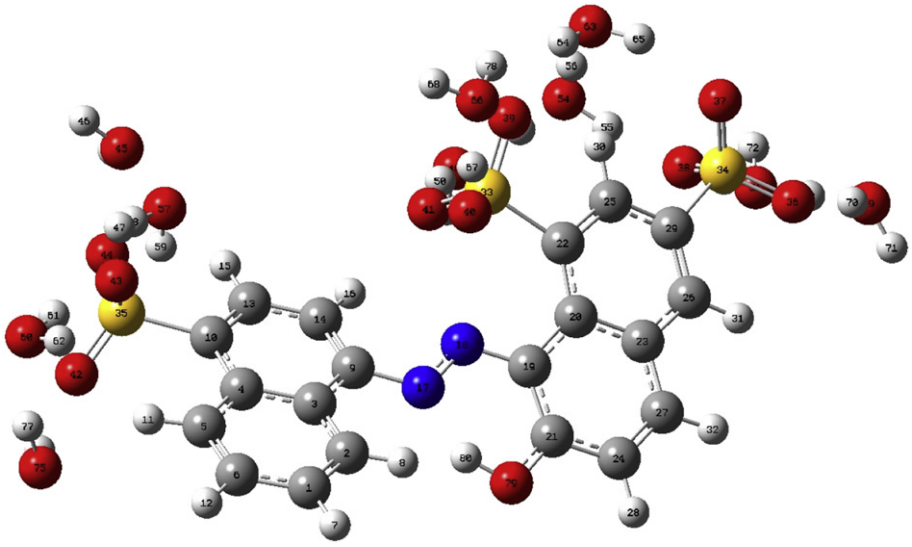

Fig. 3. Model representing a molecule of Ponceau 4R in the dissociated form ((8Z)-7-oxo-8-[(4-sulphonatonaphthalen-1-yl)hydrazinylidene]naphthalene-1,3-disulphonate), in acidic media. The dye molecule is surrounded by water molecules and H_3O^+, in a continuous dielectric defined by IEFPCM [30].

occur without reducing the organic load, and also provided information about the possible early stages of the photocatalytic degradation pathway. The DFT and TD-DFT calculations were done using Gaussian 09 [32], and the semi-empirical calculations were based on AMPAC 9.2 [33].

3. Results and discussion

3.1. Electronic spectrum

Fig. 4 presents the absorption spectrum of an aqueous solution of P4R at a concentration of 4.0×10^{-5} mol L^{-1} and pH 3.0, in the spectral range between 250 and 650 nm, and the simulated spectrum using a TD-DFT method for P4R in aqueous acid.

As suggested by the results obtained from TD-DFT calculations, the absorption bands observed experimentally for P4R are of considerable complexity, involving combinations of electronic transitions with different weights. The first two electronic transitions of the theoretical spectrum are correlated, resulting in the band with absorption maximum at 507 nm observed in the experimental absorption spectrum. The transition $S_0 \rightarrow S_1$ has an oscillator strength, *f*, equal to 0.2543, compatible with a π,π^* electronic transition. This is in agreement with the molar absorptivity at 507 nm and with the characteristics of the involved molecular orbitals (MO). The excitation wavelength calculated for this transition is 497.37 nm, with a minimal discrepancy with the value experimentally estimated, and is a consequence of the combination of four different electronic transitions (Supplementary material) involving a set of molecular orbitals, being predominant the HOMO, LUMO. The second transition that compose this absorption band ($S_0 \rightarrow S_2$) is also π,π^*, with oscillator strength and excitation wavelength respectively 0.2034 and 464.70 nm.

The second absorption band observed in the experimental absorption spectrum, with an absorption maximum estimated as 333 nm, is composed of five electronic transitions, some of low intensity. The transition $S_0 \rightarrow S_7$ is the theoretical corresponding to experimental absorption maximum of the second absorption band. This transition presents excitation wavelength and oscillator strength respectively 333.91 nm and 0.1387, being the boundary transition between the second and the third absorption band. The transition $S_0 \rightarrow S_3$ presents a very discrepant intensity, possibly an artifact created keeping in view the limitations of the model used - for example, the use of an insufficient number of discrete solvent molecules. Moreover, the use of a more representative number of discrete solvent molecules tends to become impractical as a reliable description of the system using method of quantum mechanics.

The range for the third absorption band with threshold at 243.42 nm in the theoretical spectrum, contains eighteen electronic transitions. The transition $S_0 \rightarrow S_{11}$ corresponds to the third experimental absorption maximum. The calculated excitation wavelength is equal to 294.09 nm. It is also a π,π^* transition, with an oscillator strength equal to 0.1826. The corresponding experimental absorption maximum occurs near 250 nm.

The comparison between the maximum excitation wavelengths and the corresponding experimental values shows that the deviations between the calculated values and those estimated experimentally are generally acceptable (the λ_{max} at 507 nm is about 2% higher than the calculated excitation wavelength; the discrepancy between the λ_{max} of the second band and the theoretical value is almost zero; for the third band the discrepancy is about −15%). This

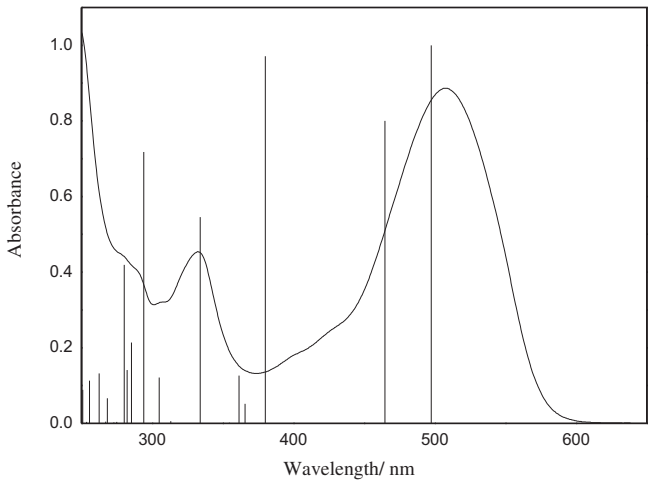

Fig. 4. Absorption spectrum of aqueous solution of P4R, $4{,}0 \times 10^{-5}$ mol L^{-1}, at pH 3. Vertical lines represent the oscillator strengths in the UV/VIS spectrum simulated for the compound, based on the applied theoretical model.

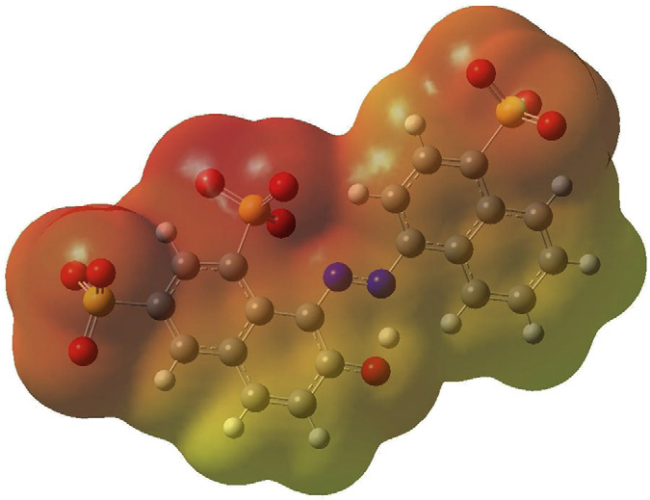

Fig. 5. Representation of the electron density from total SCF density, mapped with ESP for P4R in its dissociated form, in the ground state.

trend of increasing divergence between the theoretical and experimental data as the transition energy increases is still an intrinsic problem of DFT [34]. Considering the above analysis, the proposed model to describe theoretically the P4R in acidified aqueous solution (Fig. 4) can be considered acceptable for the purpose for which it was intended.

The electron density from total SCF density, mapped with the electrostatic potential (ESP), computed for P4R in its dissociated form is shown in Fig. 5. The electron density varies in the range between −0.35 and −0.17 electrons/bohr^3. The region with maximum electron density is precisely that which accommodates the sulphonate groups, at the top of the figure. The sulphonate group in the position 1 of the 7-hydroxynaphthalene fragment has the highest electron density, followed by the same group at position 3 of the same fragment, and the sulphonate group at position 4- of the azo-naphthalene fragment. The region with lighter shade (Fig. 5) has at least 50% of the maximum electron density presented by the region that accommodates the sulphonate groups. A similar trend is also observed for the structure in the relaxed S_1 state.

There is no region deficient in electrons in the structure, either in the ground state or in the relaxed S_1 state.

The structure of P4R in the S_1 state was optimized to provide an overview of structural changes and alterations in reactive sites after electronic excitation and relaxation of the excited state in the solvent. Structurally, there are some expressive changes in the torsion between the naphthalene groups, which tend to favor a better exposure of the C(09)-N(17) bond to the action of reactive species or even for homolytic scission (Supplementary Material and Fig. 3). In terms of changes in the reactive sites, significant variations in the Mulliken electronic charge occur between the atoms linking the two naphthalene fragments for the species in the S_1 state, compared to the structure in the ground state. The decrease in electronic charge on the atoms N(18) − 26.7% and N(17) − 8.8% was noteworthy. The increase in electronic charge on atoms C(09) − 5.7% and C(19) − 23.8%, and increased electron density of bonds formed by these atoms, was verified by shortening them. An increase of 7.3% in electronic charge on H(80) suggests an intensification of the intramolecular hydrogen bond, which tends to favor the stability of the N(18)—C(19) bond, and appears to be one of the reasons for the observed variation in the electronic charge on the atoms that form the bridge between the naphthalene fragments.

3.2. Photodecolorization in the absence of catalyst

Fig. 6 shows the progress of the dye decolorization which occurred during the direct photolysis. It should be emphasized that the observed decolorization is irreversible.

Fig. 6 – inset suggests the occurrence of two distinct pseudo-first order kinetic regimens for the decolorization via direct photolysis into the monitoring interval. The second stage of decolorization occurs at a rate almost three times higher than the first.

Since the observed P4R decolorization is an irreversible process, it is plausible to consider that during the direct photolysis decolorization and structural degradation must occur simultaneously. This is evident when the content of total organic carbon during the

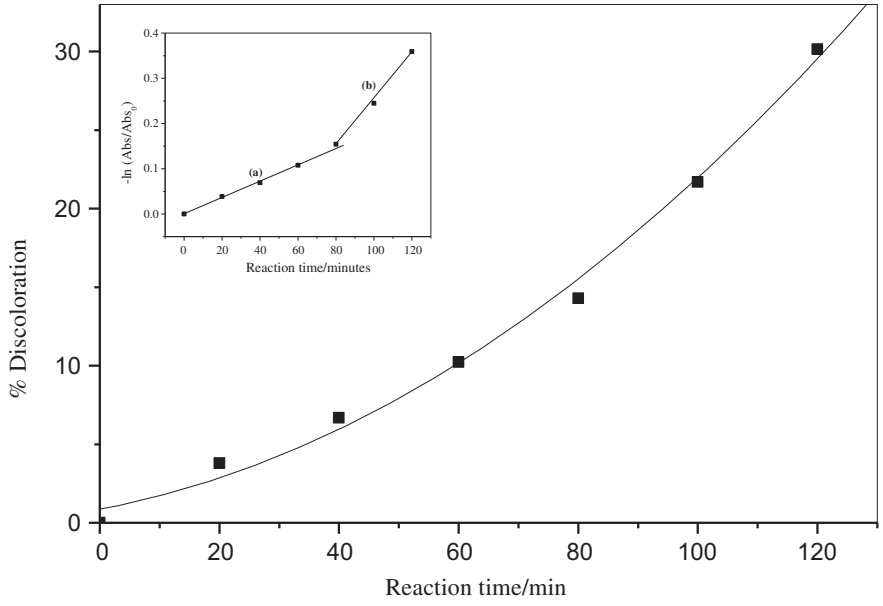

Fig. 6. Percentage of dye decolorization, monitored at 507 nm, as function of irradiation time. The reaction was induced in the absence of catalyst, using the mercury vapor lamp. In the inset is shown the two first order constants for the decolorization of Ponceau 4R: (a) $k_d = 1.89 \times 10^{-3}$ min^{-1}, $r = 0.9976$; (b) $k_d = 5.11 \times 10^{-3}$ min^{-1}, $r = 0.9977$.

decolorization is monitored. Although the decolorization did not lead to dye mineralization, this resulted in a partial structural degradation without reduction of the organic load, as shown in Fig. 7.

If, during the direct photolysis, decolorization occurs simultaneously with the partial degradation of the original structure, the photochemically induced homolytic cleavage of certain bonds, followed by secondary oxidative reactions, is a plausible pathway for this process. An initiation via chemical reactions triggered via reactive oxygen species (ROS) is highly unlikely. Oxidation processes with the participation of molecular oxygen in the ground state tend to be extremely slow due to electron spin restrictions. Chemical reactions triggered directly from the S_1 state of P4R are unlikely, since this state being π,π^* in nature should not have a lifetime sufficiently long to enable them. With respect to the triplet state adjacent to S_1, both states have equivalent orbital symmetry (Supplementary Material) [35]. So it is very unlikely that intersystem crossing is an efficient process. Thus, reactions involving the action of ROS produced from the T_1 (π,π^*) state, or even between ROS and this state should also be discarded.

Estimates made using the semi-empirical PM6 model considering the homolytic cleavage of C(9)–N(17), N(17)–N(18) and N(18)–C(19) bonds suggest that cleavage of C(9)–N(17) of P4R in the S_1 state may be the preferred route for the primary stage of degradation promoted by a photolytic route. The minimum energy required to promote this cleavage is 180 kJ/mol, corresponding to photons of 660 nm. The energy estimated for the S_1 relaxed state, 112.33 kJ/mol (1064.95 nm), is insufficient to promote the cleavage of this bond. The same scission from S_0 requires about 466 kJ/mol.

For the C(19)–N(18) bond, the minimum energy to promote the homolytic cleavage is about 220 kJ/mol for P4R in the S_1 state, while for the species in the S_0 state this value is about 305 kJ/mol. In the case of the N(17)–N(18) bond, the values are respectively 502 kJ/mol and 460 kJ/mol, for the electronically excited P4R, and P4R in the ground state. Importantly, the radiation incident on the experimental setup of this study provides energy to the reaction medium in a wide spectral range from 295 nm.

3.3. Photocatalytic degradation of P4R

For photocatalytic processes, a much more complex mechanism must be expected, combined with the homolytic cleavage by direct photolysis, being the main reactions derived from the processes induced by photocatalysis, involving reactive species produced in the active sites of the excited catalyst due to adsorption-desorption processes involving species in solution or suspension and the catalyst surface [7,36]. As result, the degradation of P4R can occur in a relatively short time, depending on the performance of the photocatalyst, and may even result in the complete mineralization of the dye.

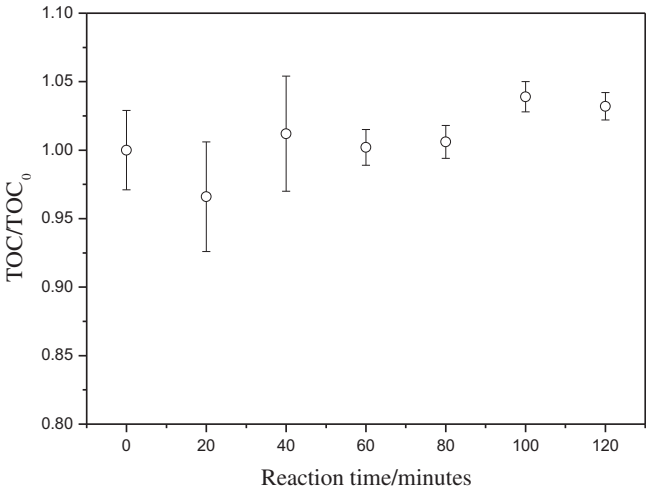

Fig. 7. Relationship between the normalized total organic carbon content (TOC/TOC_0) and the irradiation time for the photolysis of P4R in aqueous solution at pH 3 in the absence of catalyst.

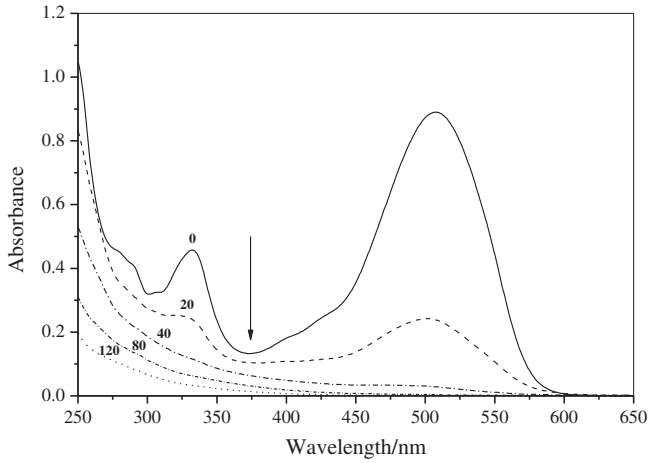

Fig. 8. Behavior of the absorption spectrum of a solution of Ponceau 4R at pH = 3 during a photocatalytic reaction (time in minutes), mediated by TiO_2 P25, using a 400 W high pressure mercury vapor lamp as radiation source.

Fig. 8 shows the temporal behavior of the absorption spectrum of an aqueous solution of P4R at pH3, during decolorization mediated by TiO_2 P25.

Similar to the observed in the direct photolysis, two distinct pseudo-first order kinetic regimens were observed for the decolorization of P4R during the photocatalytic process (Table 1). Unlike other photocatalysts, the second rate estimated for the decolorization of TiO_2 P25 was lower than the first. An exception occurs in the decolorization promoted by the composite TiO_2/ZnPc 1.6% where only one rate constant was verified.

Data from Table 1 and Fig. 9 suggest that, among the photocatalysts studied, the composite TiO_2/ZnPc 1.6% has an efficiency of decolorization close to that estimated for TiO_2 P25 Degussa, which showed the best result, followed by the TiO_2 sol–gel TX. In the presence of TiO_2 P25 or the composite TiO_2/ZnPc 1.6%, a solution containing P4R reached 100% of decolorization after 80 min of irradiation. In the photocatalytic process mediated by TiO_2 Sol–Gel TX, the same 100% of decolorization was achieved after 120 min of irradiation.

On the performance of the photocatalysts obtained by the Pechini method in promoting the decolorization of P4R, it was systematically lower than that observed by the catalysts presented above. The photocatalysts synthesized by the Pechini method were,

Table 1
Apparent P4R decolorization rates induced by the studied catalysts.

Catalyst	Apparent decolorization rate ($\times 10^2$ min^{-1})
Direct photolysis, without catalyst	0.19;0.51
TiO_2 Pechini 1:2:8	0.56;2.05
TiO_2 Pechini 1:4:16	0.67;1.39
TiO_2 Pechini 1:8:32	1.04;1.88
TiO_2 Sol–Gel TX	3.16;5.90
TiO_2/FtZn 1.6%	5.39
TiO_2 P25	5.97;1.11

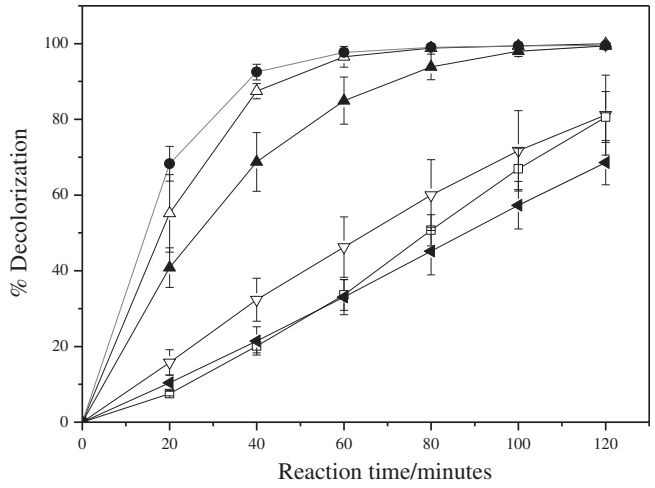

Fig. 9. Decolorization of a solution of P4R obtained by photocatalysis promoted by different catalysts: TiO_2 P25 Degussa (●); TiO_2/ZnPc 1.6% (Δ); TiO_2 sol–gel TX (▲); TiO_2 Pechini 1:8:32 (▽); TiO_2 Pechini 1:2:8 (□); TiO_2 Pechini 1:4:16 (◂).

by extrapolation, able to promote the complete decolorization of the P4R solution after 173, 180 and 190 min, respectively for TiO_2 Pechini 1:8:32, 1:4:16, and 1:2:8.

Fig. 10 shows the typical kinetic behavior for the photocatalytic degradation of P4R, monitored by the decrease in TOC content.

It is well accepted that the heterogeneous photocatalytic degradation of organic matter usually follows Langmuir–Hinshelwood kinetics [13,27]. As the amount of dye in the model-effluent is low (10^{-5} mol dm^{-3}) and the concentration of reactive species produced during the adsorption-desorption process on the electronically excited surface of the catalyst must quickly reach a stationary-state regimen after the beginning of the reaction, the behavior of the apparent degradation rate depicts pseudo-first order kinetics [27]. These reactive species should preferably be produced from other species present in the reaction medium, such as oxygen, water or ionized species, more mobile than the P4R. As a result, the degradation of P4R must involve preferentially the action of the desorbed active species, occurring mainly in the catalyst-solution interface. Moreover, as the reaction proceeds, the remaining P4R must still compete with its degradation products, of higher mobility, for active sites on the excited surface of the catalyst.

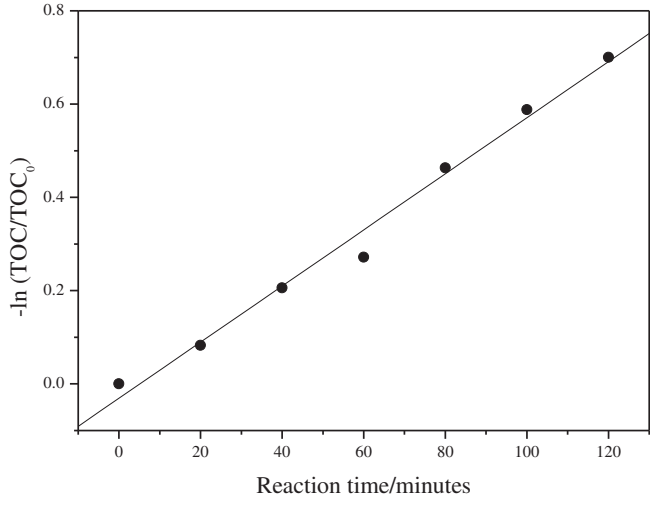

Fig. 10. Typical kinetics obtained for the mineralization of P4R, using the composite TiO_2/ZnPc 1.6%. The average deviation in the measurements was around 3%.

Experiments involving the adsorption–desorption equilibrium of aqueous solutions of P4R in the dark, at pH3 and 298 K, using the catalysts evaluated in this study (results not shown), suggest that for TiO_2 P25 and TiO_2/ZnPc this equilibrium is established with a fraction slightly higher than 2.0% of the P4R initially present in solution, whereas for TiO_2 Pechini 1:2:4,1:4:16 and 1:8:32 this equilibrium was established with a fraction lower than 1.0%. For TiO_2 Sol–Gel, the equilibrium was reached with 1.0% of the P4R initially present in solution. In all cases, the adsorption-desorption equilibrium was reached 20 min after the preparation of suspensions – time equivalent to the consumed between preparation of the suspensions and the beginning of the irradiations. Regardless of differences in the specific areas of the catalysts, the adsorbed fraction remained practically unchanged throughout the rest of the experiment, except for TiO_2 Sol–Gel for which a new equilibrium adsorption-desorption began to settle 20 min before the end of the experiment, with an increase in the fraction of adsorbed P4R. It was considered for these essays the same time interval used in the experiments of photocatalysis.

As the photocatalytic reactions occur at temperatures higher than 298 K and considering the adsorption-desorption dynamics and degradation of P4R, it is likely that its fraction in equilibrium with the electronically excited surface of the catalyst be much lower than estimated in adsorption–desorption experiments mentioned above.

Analysis of data obtained from TOC measurements (Table 2) shows that the performance of the composite in mineralization of P4R is almost three times higher than those presented by P25 TiO_2, and still much higher than that presented by the other catalysts evaluated in this study. About 50% of the organic matter was mineralized after 120 min of reaction mediated by the composite. Under similar conditions, in the degradation mediated by TiO_2 P25 18% mineralization was reached, while for TiO_2 Pechini 1:4:16, TiO_2 1:8:32 Pechini and TiO_2 Sol–Gel TX a level of mineralization between 14 and 15% was reached.

Although TiO_2/ZnPc 1.6% has shown high performance in the mineralization of P4R using artificial radiation, very likely because the source of radiation used also provides components in the visible spectrum [14]. Even so, it is expected that the result is much better under solar irradiation. This composite is part of a set of catalysts developed with the aim of broadening the range of solar radiation capable to trigger heterogeneous photocatalytic processes mediated by solar light [14]. Previous results show that these composites have a superior performance to that presented by TiO_2 P25 and other catalysts based on TiO_2 in photocatalytic processes mediated by solar radiation [14,27,37,38].

The photocatalytic activity of TiO_2/ZnPc 1.6% seems to be a result of synergism between the photocatalytic characteristics inherent to TiO_2 P25, combined with the redox properties and charge transport

Table 2
Percentage of mineralization and apparent mineralization rate induced by the studied catalysts on P4R after 120 min of photolysis.

Catalyst	Mineralization after 120 min of photolysis (%)	Apparent mineralization rate ($\times 10^3$ min^{-1})
Direct photolysis, without catalyst	0.0	0.00
TiO_2 Pechini 1:2:8	4.4	0.39
TiO_2 Pechini 1:4:16	14.1	1.47
TiO_2 Pechini 1:8:32	14.2	0.95
TiO_2 Sol–Gel TX	15.1	1.30
TiO_2 FtZn 1.6%	50.4	6.02
TiO_2 P25	18.2	2.03

capabilities of the ZnPc Frenkel's "J" aggregates on the semiconductor surface [14,38–40]. When electronically excited, these aggregates are able to inject photo-electrons into the conduction band of semiconductor oxide, causing an increase in the concentration of electrons and inducing an increase in the concentration of reactive oxygen species (ROS) capable of degrading organic matter.

Studies involving scanning tunneling microscopy of different metal phthalocyanines confirm that the above mentioned aggregates are adsorbed onto the semiconductor surface [41]. Machado and coworkers have reported that the presence of ZnPc aggregates on the surface of TiO_2 apparently did not cause distortions in its crystalline structure [14].

The photocatalytic efficiency of a semiconductor oxide is the result of combining a number of factors, including the method of synthesis [13,42]. TiO_2 Pechini 1:2:8, for example, was the catalyst that had the lowest performance in the degradation of P4R, with mineralization just over 4% after 120 min of reaction. Although the route of synthesis is similar to the other two catalysts prepared by Pechini method, for this oxide titanium tetraisopropoxide was used in much higher proportion compared to the other reagents. One explanation for the observed difference in performance is that the stoichiometric relationship between titanium tetraisopropoxide and the other species used to form the polymeric resin did not guarantee high homogeneity in the dispersion of metal ions, inducing the formation of crystalline defects in the semiconductor oxide, very likely committing the number of active sites on the surface of the catalyst, capable of producing active species, jeopardizing its photocatalytic activity, since that crystalline defects favor the recombination of electrons and holes, leading to poor photoactivity [43–46]. For the other oxides prepared by the Pechini method the molar ratios employed in the synthesis were more favorable. As a result, the lower photocatalytic efficiency of TiO_2 Pechini 1:2:8 was not observed in these or occurred to a lesser extent.

Although not the only parameter to be considered, the pH control of the reaction medium had a positive influence on the overall efficiency of a photocatalytic process [7,13,42]. For the model-effluent containing P4R, the pH of the reaction medium, adjusted below pH_{zpc} of pure anatase, around 4 [17], and TiO_2 P25 – and very likely for the composite – equal to 6.25 [7,13], provides the dye with a net negative net charge (Fig. 5) which tends to favor its interaction with the surface of the catalysts, facilitating the action of the desorbed active species, which can ensure a higher degradability for the organic substrate. Similar trend was observed in previous studies on the photocatalytic degradation of a lignosulphonate in aqueous solution, where the degradation efficiency was higher when the initial pH of the reaction medium was adjusted below 4 [27].

The specific surface area (SSA) is generally correlated to the availability of active sites on the catalyst surface. Although both the TiO_2 P25 and TiO_2/ZnPc 1.6% have the same ratio between anatase and rutile, the SSA of the composite is 23% lower than that of TiO_2 P25 (Table 3). Most likely, this difference is a result of the incorporation of ZnPc aggregates on the surface of the semiconductor. However, an enhanced photocatalytic activity not only depends on the specific surface area, but several other parameters such as surface acidity, control of the recombination process, interfacial electron-transfer rate, among others [13,42,47]. For the composite under study, the surface sensitization by electron transfer via physisorbed ZnPc [14] should compensate the decrease in surface area, increasing the efficiency of the photocatalytic process. It should be emphasized that the extended range of wavelengths, shifted to the visible region of the electromagnetic spectrum, capable of positively influencing the electron transfer between the excited dye and the semiconductor conduction band tends to improve electron–hole separation [14,42,48–52].

Quantifying the fraction of anatase was based on X-Ray diffraction (XRD) measurements (Supplementary materials). For all photocatalysts, especially those synthesized in this study anatase predominated, the polymorph that usually has the highest photoactivity [13,53,54]. The results suggest an inverse relationship between the percentage of anatase and the degree of mineralization achieved (Tables 2 and 3). This trend excludes the TiO_2 Pechini 1:2:8, which has the lowest performance in the degradation of P4R, although it has the second lowest percentage of anatase in the set of catalysts studied. As discussed above, the occurrence of crystalline defects in the structure of TiO_2 Pechini 1:2:8 should be the reason for behavior outside of the trend observed for this catalyst. These defects may be related to the fraction of rutile, formed in much larger proportion, and a possible orientation of these crystals on the surface of the particles, as suggested by the displacement of the diffraction peak associated with crystalline phases in the diffractograms (Supplementary materials).

3.4. Quantum yield of hydroxyl radical generation ($\Phi_{HO^\bullet}$)

The quantum yield of hydroxyl radical generation ($\Phi_{HO^\bullet}$) has been considered to be a reliable parameter to quantify the photocatalytic activity of a catalyst. However, the $\Phi_{HO^\bullet}$ estimated in this work for TiO_2/ZnPc 1.6%, equal to 2%, is three times smaller than the estimated value for TiO_2 P25 [14,55], although the photocatalytic activity of the composite in the mineralization P4R was almost three times higher than the verified with the use of TiO_2 P25. Recent results on the degradation of another organic substrate (paracetamol) mediated by this compound in aqueous media indicated a similar trend [38]. These results suggest that the premise that $\Phi_{HO^\bullet}$ is a reliable quantitative parameter of the photocatalytic activity of a catalyst is not valid at least for the class of composites studied in this work. Most likely, the photoelectrons injected from ZnPc excitons into the TiO_2 conduction band are the reason for this behavior. These photoelectrons should amplify the importance of processes mediated by superoxide anion-radicals and other electron-rich reactive species generated from the TiO_2 conduction band that begin to compete with hydroxyl radicals in the reactions that can lead to mineralization of the substrate under study. Therefore, at least for the TiO_2/ZnPc composites or other photocatalysts able to increase injection of photoelectrons into the conduction band of a photocatalytically active semiconductor oxide, $\Phi_{HO^\bullet}$ is not a reliable parameter to evaluate the photocatalytic activity of a catalyst.

Table 3
Specific surface area (SSA) and fraction of anatase for the photocatalysts studied.

Photocatalyst	SSA_{BET} ($m^2\,g^{-1}$)	% Anatase
TiO_2 Pechini 1:2:8	35	84
TiO_2 Pechini 1:4:16	40	91
TiO_2 Pechini 1:8:32	63	99
TiO_2 Sol–Gel TX	30	87
TiO_2/FtZn 1.6%	40	70
TiO_2 P25	52	70

4. Conclusions

The theoretical model proposed to represent the solvated P4R in acidic medium suggests that this compound tends to be degraded via a photoinduced homolytic cleavage of C(9)–N(17) and N(18)–C(19) bonds, in combination with reactions triggered and mediated in the electronically excited surface of the catalyst, supporting the results obtained from the direct photolysis.

Among the catalysts studied, the composite TiO_2/ZnPc 1.6% presented the best photocatalytic performance, followed by TiO_2

P25, and TiO_2 Sol–Gel TX, respectively producing 50%, 18% and 15% of mineralization of P4R after 120 min of reaction. Among the oxides obtained via the Pechini method, TiO_2 Pechini 1:4:16 and TiO_2 Pechini 1:8:32 present comparable photocatalytic performances with a mineralization of P4R around 14%, whereas TiO_2 Pechini 1:2:8 presented the lowest performance, about 4%, attributed to an unfavorable stoichiometric relationship between titanium tetraisopropoxide and the other reagents during its synthesis.

The highest photocatalytic activity of TiO_2/ZnPc 1.6% seems to be the result of synergism between the photocatalytic characteristics inherent to TiO_2 P25 with the redox properties and charge transport of ZnPc Frenkel's "J" aggregates on the semiconductor surface. The sensitization of TiO_2 P25, induced by zinc phthalocyanine aggregates was effective in producing a more active catalyst.

At least for the composite TiO_2/ZnPc 1.6%, $\Phi_{HO^\bullet}$ is not a valid parameter for the reliable estimation of the photocatalytic activity, probably due to the action of ZnPc, injecting photo-electrons in TiO_2 conduction band. These photo-electrons should amplify the importance of other processes that begin to compete with hydroxyl radicals in the reactions that can lead to mineralization of the substrate under study.

Acknowledgments

The authors are grateful to CNPq, INCT/INFo, FAPEMIG and CAPES by the financial support and scholarships. To Laboratório de Caracterização de Catalisadores, Faculdade de Engenharia Química da Universidade Federal de Uberlândia by BET analysis of the catalysts. To Nanobrax for providing some of the catalysts employed in this study.

Appendix. Supplementary data

Supplementary data associated with this article can be found in the online version, at doi:10.1016/j.dyepig.2011.06.007.

References

[1] Ohno T, Tokieda K, Higashida S, Matsumura M. Synergism between rutile and anatase TiO_2 particles in photocatalytic oxidation of naphthalene. Applied Catalysis A: General 2003;244:383–91.
[2] Sun L, Bolton J. Determination of the quantum yield for the photochemical generation of hydroxyl radicals in TiO_2 suspensions. The Journal of Physical Chemistry 1996;100:4127–34.
[3] Palmisano G, Augugliaro V, Pagliaro M, Palmisano L. Photocatalysis: a promising route for 21st century organic chemistry. Chemical Communications 2007;33:3425–37.
[4] Shahmoradi B, Ibrahim IA, Sakamoto N, Ananda S, Row TNG, Soga K, et al. Surface modification of molybdenum-doped organic-inorganic hybrid TiO_2 nanoparticles under hydrothermal conditions and treatment of pharmaceutical effluent. Environmental Technology 2010;31:1213–20.
[5] Reife A, Freeman H. Environmental chemistry of dyes and pigments. New York: Wiley-Interscience; 1996.
[6] Vautier M, Guillard C, Herrmann J-M. Photocatalytic degradation of dyes in water: case study of indigo and indigo carmine. Journal of Catalysis 2001;201:46–59.
[7] Chong MN, Jin B, Chow CWK, Saint C. Recent developments in photocatalytic water treatment technology: a review. Water Research 2010;44:2997–3027.
[8] Fernandez J, Maruthamuthu P, Kiwi J. Photobleaching and mineralization of Orange II by oxone and metal-ions involving Fenton-like chemistry under visible light. Journal of Photochemistry and Photobiology A: Chemistry 2004;161:185–92.
[9] Alinsafi A, Evenou F, Abdulkarim EM, Pons MN, Zahraa O, Benhammou A, et al. Treatment of textile industry wastewater by supported photocatalysis. Dyes and Pigments 2007;74:439–45.
[10] Machado AEH, Xavier TP, Souza DR, Miranda JA, Duarte ETFM, Ruggiero R, et al. Solar photo-Fenton treatment of chip board production waste water. Solar Energy 2004;77:583–9.
[11] Mahmoodi NM, Arami M, Limaee NY, Gharanjig K, Ardejani FD. Decolorization and mineralization of textile dyes at solution bulk by heterogeneous nanophotocatalysis using immobilized nanoparticles of titanium dioxide. Colloids and Surfaces A: Physicochemical and Engineering Aspects 2006;290:125–31.
[12] Silva CG, Wang W, Faria JL. Photocatalytic and photochemical degradation of mono, di- and tri-azo dyes in aqueous solution under UV irradiation. Journal of Photochemistry and Photobiology A: Chemistry 2006;18:314–24.
[13] Hoffman MR, Martin ST, Choi W, Bahnemann DW. Environmental applications of semiconductor photocatalysis. Chemical Reviews 1995;95:69–96.
[14] Machado AEH, França MD, Velani V, Magnino GA, Velani HMM, Freitas FS, et al. Characterization and evaluation of the efficiency of TiO_2/Zinc phthalocyanine nanocomposites as photocatalysts for wastewater treatment using solar irradiation. International Journal of Photoenergy; 2008. doi:10.1155/2008/482373. Article ID 482373.
[15] Pascoal SA, Lima CAP, Sousa JT, Lima GGC, Vieira FF. Aplicação de radiação UV artificial e solar no tratamento fotocatalítico de efluentes de curtume. Química Nova 2007;30:1082–7.
[16] Mills A, Le Hunte S. An overview of semiconductor photocatalysis. Journal of Photochemistry and Photobiology A: Chemistry 1997;108:1–35.
[17] Vohra MS, Tanaka K. Enhanced photocatalytic activity of nafion-coated TiO_2. Environmental Science & Technology 2001;35:411–5.
[18] Sugimoto T. Underlying mechanisms in size control of uniform nanoparticles. Journal of Colloid and Interface Science 2007;309:106–18.
[19] Kudo A, Niishiro R, Iwase A, Kato H. Effects of doping of metal cations on morphology, activity, and visible light response of photocatalysts. Chemical Physics 2007;339:104–10.
[20] Batista PS. Propriedades morfológicas e estruturais e rendimento quântico de geração de radicais hidroxila em amostras sintetizadas de dióxido de titânio. Ph.D. Thesis. Uberlândia, Brazil:Universidade Federal de Uberlândia; 2010.
[21] Sharma GD, Mathur SC, Dube DC. Organic photovoltaic solar cells based on some pure and sensitized dyes. Journal of the Materials Science 1991;26:6547–52.
[22] Krüger J, Plass R, Cevey L, Piccirelli M, Grätzel M, Bach U. High efficiency solid-state photovoltaic device due to inhibition of interface charge recombination. Applied Physics Letters 2001;79:2085–8.
[23] Rehm JM, McLendon GL, Nagasawa Y, Yoshihara K, Moser J, Grätzel M. Femtosecond electron-transfer dynamics at a sensitized dye-semiconductor (TiO_2) interface. The Journal of Physical Chemistry 1996;100:9577–8.
[24] FDA. Compliance program guidance manual. http://www.fda.gov/downloads/Food/GuidanceComplianceRegulatoryInformation/ComplianceEnforcement/ucm073305.pdf [accessed December 2010], 10.
[25] Ponceau 4R. http://en.wikipedia.org/wiki/E124 [accessed December 2010].
[26] EFSA. Scientific opinion on the re-evaluation of Ponceau 4R (E 124) as a food additive. http://www.efsa.europa.eu/en/scdocs/scdoc/1328.htm [accessed December 2010].
[27] Machado AEH, Miranda JA, Freitas RF, Duarte ETFM, Ferreira LF, Albuquerque YDT, et al. Destruction of the organic matter present in effluent from a cellulose and paper industry using photocatalysis. Journal of Photochemistry and Photobiology A: Chemistry 2003;155:231–41.
[28] Gao R, Stark J, Bahnemann DW, Rabani J. Quantum yields of hydroxyl radicals in illuminated TiO_2 nanocrystallite layers. Journal of Photochemistry and Photobiology A: Chemistry 2002;148:387–91.
[29] Cassaignon S, Kolesh M, Jolivet J-P. Selective synthesis of brookite, anatase and rutile nanoparticles: thermolysis of $TiCl_4$ in aqueous nitric acid. Journal of the Materials Science 2007;42:6689–95.
[30] Tomasi J, Mennucci B, Cammi R. Quantum mechanical continuum solvation models. Chemical Reviews 2005;105:2999–3094.
[31] Grensemann H, Gmehling J. Performance of a conductor-like screening model for real solvents model in comparison to classical group contribution methods. Industrial & Engineering Chemistry Research 2005;44:1610–24.
[32] Frisch MJ, Trucks GW, Schlegel HB, Scuseria GE, Robb MA, Cheeseman JR, et al. Gaussian 09, revision B.01. Wallingford CT: Gaussian, Inc; 2010.
[33] AMPAC 9.2.1. KS, USA: Semichem, Inc; 2008.
[34] Cai Z-L, Sendt K, Reimers JR. Failure of density-functional theory and time-dependent density-functional theory for large extended π systems. Journal of Chemical Physics 2002;117:5543–9.
[35] Turro NJ, Ramamurthy V, Scaiano JC. Modern molecular photochemistry of organic molecules. 1st ed. Sausalito, Ca: University Science Books; 2010.
[36] Fujishima A, Zhang X, Tryk DA. TiO_2 photocatalysis and related surface phenomena. Surface Science Reports 2008;63:515–82.
[37] Duarte ETFM, Jung C, Machado AEH, Miranda JA, Oliveira L, Sattler C, et al. Construção e estudos de perfomance de um reator fotoquímico tipo CPC ("Compound Parabolic Concentrator"). Química Nova 2005;28:921–6.
[38] Machado AEH, França MD, Batista PS, Menezes VH, Tiago FS, Oliveira DFM. unpublished results.
[39] Fidder H, Knoester J, Wiersma DA. Optical properties of disordered molecular aggregates: a numerical study. Journal of Chemical Physics 1991;95:7880–91.
[40] Kim O-K, Je J, Jernigan G, Buckley L, Whitten D. Super-helix formation induced by cyanine J-aggregates onto random-coil carboxymethyl amylose as template. Journal of the American Chemical Society 2006;128:510–6.
[41] Qiu XH, Nazin GV, Ho W. Mechanisms of reversible conformational transitions in a single molecule. Physical Review Letters 2004;93. Article ID 196806.
[42] Carp O, Huisman CL, Reller A. Photoinduced reactivity of titanium dioxide. Progress in Solid State Chemistry 2004;32:33–177.
[43] Tanaka K, Capule MFV, Hisanaga T. Effect of crystallinity of TiO_2 on its photocatalytic action. Chemical Physics Letters 1991;187:73–6.
[44] Saadoun L, Ayllón JA, Jimànez-Becerril J, Peral J, Domènech X, Rodríguez Clemente R. 1,2-Diolates of titanium as suitable precursors for the preparation

of photoactive high surface titania. Applied Catalysis B: Environmental 1999; 21:269–77.
[45] Zhang ZB, Wang CC, Zakaria R, Ying JY. Role of particle size in nanocrystalline TiO_2 – based photocatalysts. The Journal of Physical Chemistry B 1998;102: 10871–8.
[46] Yin H, Wada Y, Kitamura T, Kambe S, Murasawa S, Mori H, et al. Hydrothermal synthesis of nanosized anatase and rutile TiO_2 using amorphous phase TiO_2. Journal of Materials Chemistry 2001;11:1694–703.
[47] Furube A, Asahi T, Masuhara H, Yamashita H, Anpo M. Direct observation of a picosecond charge separation process in photoexcited platinum-loaded TiO_2 particles by femtosecond diffuse reflectance spectroscopy. Chemical Physics Letters 2001;336:424–30.
[48] Wang C-Y, Liu C-Y, Wang W-Q, Shen T. Photochemical events during the photosensitization of colloidal TiO_2 particles by a squaraine dye. Journal of Photochemistry and Photobiology A: Chemistry 1997;109:159–64.
[49] Shourong Z, Qingguo H, Jun Z, Bingkun W. A study on dye photoremoval in TiO_2 suspension solution. Journal of Photochemistry and Photobiology A: Chemistry 1997;108:235–8.
[50] Zhang F, Zhao J, Zang L, Shen T, Hidaka H, Pelizzetti E, et al. Photoassisted degradation of dye pollutants in aqueous TiO_2 dispersions under irradiation by visible light. Journal of Molecular Catalysis A: Chemistry 1997;120:173–8.
[51] Zhang F, Zhao J, Zang L, Shen T, Hidaka H, Pelizzetti E, et al. TiO_2-assisted photodegradation of dye pollutants II. Adsorption and degradation kinetics of eosin in TiO_2 dispersions under visible light irradiation. Applied Catalysis B: Environmental 1998;15:147–56.
[52] Kiriakidou F, Kondarides DI, Verykios XE. The effect of operational parameters and TiO_2-doping on the photocatalytic degradation of azo-dyes. Catalysis Today 1999;54:119–30.
[53] Diebold U. The surface science of TiO_2. Surface Science Reports 2003;48:53–229.
[54] Tryba B, Toyoda M, Morawski AW, Nonaka R, Inagaki M. Photocatalytic activity and OH radical formation on TiO_2 in the relation to crystallinity. Applied Catalysis B: Environmental 2007;71:163–9.
[55] Wang C-Y, Rabani J, Bahnemann DW, Dohrmann JK. Photonic efficiency and quantum yield of formaldehyde formation from methanol in the presence of various TiO_2 photocatalysts. Journal of Photochemistry and Photobiology A: Chemistry 2002;148:169–76.